





## 22 **Abstract**

23 Dust is an important aerosol affecting air quality in China in winter and spring that  
24 is potentially influenced by the interannual climate variability associated with El Niño.  
25 Here, the impacts of El Niño with different temporal and spatial types on dust pollution  
26 in winter and spring in China and the potential mechanisms are investigated using an  
27 state-of-the-art earth system model (E3SMv1). We find that the Eastern Pacific (EP)  
28 and Central Pacific (CP) El Niño both increase wintertime dust concentrations by 5–50  
29  $\mu\text{g m}^{-3}$  over central-eastern China. Due to a stronger wind and lower relative humidity,  
30 which favor dust emissions near sources, and a strengthened northwesterly and reduced  
31 precipitation, which are conducive to dust transport, dust concentrations during the CP  
32 El Niño are 5–20  $\mu\text{g m}^{-3}$  higher in northern China than during the EP El Niño. El Niño  
33 with a short duration (SD) increases winter dust concentrations by 20–100  $\mu\text{g m}^{-3}$  over  
34 northern China relative to the climatological mean, while there is a decrease of 5–50  
35  $\mu\text{g m}^{-3}$  during the long duration (LD) El Niño, which are also related to the El Niño-  
36 induced changes in atmospheric circulation, precipitation, and relative humidity. In the  
37 following spring season, all types of El Niño events enhance dust over the northern  
38 China, but only the increase during the LD El Niño is statistically significant,  
39 suggesting that the weaker intensity but longer duration of the LD El Niño events can  
40 significantly affect spring dust in China. Our results contribute the current knowledge  
41 of the influence of El Niño on dust pollution, which have profound implications for air  
42 pollution control and dust storm prediction.



## 43 1. Introduction

44 Dust, one of the most important types of natural aerosols, has significant impacts  
45 on Earth's radiative balance (Seinfeld et al., 2004), regional and global climate (Kok et  
46 al, 2018; Yang et al., 2017), the hydrological cycle (Huang et al., 2014), agricultural  
47 production (Sivakumar, 2005), public health and transportation activities (Goudie,  
48 2014). The Gobi Desert and the Taklamakan Desert in northwestern China are  
49 important contributors to dust concentrations in East Asia and even globally, and about  
50 30% of the dust from the sources in China can be transported to the downwind areas  
51 over long distances (Chen et al., 2017). Despite China's vigorous efforts to combat  
52 desertification since the beginning of 21<sup>st</sup> century, strong and widespread dust storms  
53 still occurred in China in recent years (Yin et al., 2021). Therefore, a deeper and more  
54 scientific comprehension of the factors affecting dust aerosols in China is urgently  
55 needed for the early warning and mitigation of dust pollution.

56 In recent years, the influence of meteorological conditions on dust pollution in  
57 China has attracted considerable attention (Guo et al., 2019; Li et al., 2020; Lou et al.,  
58 2016; Shi et al., 2021; Yin et al., 2021; Zhu et al., 2008). Under global warming in  
59 recent decades, dust emissions and the frequency of dust storms in northern China  
60 decreased (Shi et al., 2021), which was attributed to the reduced frequency and intensity  
61 of Mongolian cyclones, related to the weakened westerly jet stream and atmospheric  
62 pressure in northern China and Mongolia, in a warming climate (Zhu et al., 2008). Due  
63 to a combination of changes in disruptive temperature anomalies in the Mongolian dust  
64 source region, the occurrence of super Mongolian cyclone, and the anomalies of sea ice  
65 in the Barents and Kara Sea and sea surface temperature (SST) in the east Pacific and  
66 northwest Atlantic, China experienced the strongest dust pollution in spring 2021 (Yin  
67 et al., 2021). Lou et al. (2016) pointed out that springtime dust concentrations exhibited  
68 a significant negative correlation with the East Asian Monsoon Index over most of  
69 China with a correlation coefficient of  $-0.64$  in their model simulations, and they found  
70 that anomalous northwesterly winds in weak East Asian monsoon years led to a strong  
71 dust transport from Mongolia to China. Mao et al. (2011) illustrated that the negative  
72 (positive) phase of Arctic Oscillation (AO) can lead to an increase (decrease) in the  
73 frequency of dust storms in northern China due to the increase (decrease) in the  
74 frequency of cold air outbreak over Mongolia.

75 El Niño-Southern Oscillation (ENSO) is a well-known mode of climate variability



76 generated by coupled ocean-atmosphere interactions that can exert a far-reaching  
77 impact on global climate despite its origin in the tropical Pacific Ocean (Trenberth,  
78 1997; Yang et al., 2016a, 2016b; Zeng et al., 2021). Numerous studies have  
79 demonstrated that El Niño can affect dust emission and transport by modulating large-  
80 scale atmospheric circulation, precipitation and temperature (Lee et al., 2015; Li et al.,  
81 2021). Using observational data over 1961–2002, Lee et al. (2015) found that the under  
82 the negative AO phase, frequency of spring dust events in northern China during El  
83 Niño was 30% higher than that during La Niña years. Li et al. (2021) used dust surface  
84 concentration data (1982–2019) from MERRA-2 reanalysis to study the impacts of  
85 ENSO events on global atmospheric dust loading and found that dust concentrations  
86 were positively correlated with Southern Oscillation Index (SOI, a consistently  
87 negative SOI is El Niño and the opposite is La Niña) over northwestern China, which  
88 suggests that El Niño was associated with a decrease in dust concentrations. Modeling  
89 studies driven by reanalysis data also revealed a relatively weak positive relationship  
90 between SOI and dust emissions over Gobi Desert, although this correlation has a large  
91 spatiotemporal variation (Gong et al., 2006; Hara et al., 2006). These numerical studies  
92 used regional models driven by or nudged to reanalysis meteorological fields, which  
93 could be influenced by factors other than El Niño. Recent studies have indicated that  
94 the El Niño impact on air pollutants can be better represented by the superposed SST  
95 perturbation method (Yu et al., 2019; Zhao et al., 2018; Zeng et al., 2021), considering  
96 the influence of ENSO alone. To the best of our knowledge, no study has yet used this  
97 approach to investigate the relationship between El Niño and dust pollution in China.

98 Additionally, previous studies mainly focused on the influences of general El Niño  
99 on dust over China, while El Niño can be classified into different temporal types (e.g.,  
100 short duration (SD) and long duration (LD) El Niño; Guo and Tan, 2018) and spatial  
101 types (e.g., East Pacific (EP) and Central Pacific (CP) El Niño; Kao and Yu, 2009).  
102 During different spatial and temporal types of El Niño, patterns of precipitation and  
103 atmospheric circulation are also different in China (Yu et al., 2019; Zeng et al., 2021),  
104 and they could have distinct effects on wintertime and springtime dust pollution in  
105 China. Nevertheless, most of the existing studies have focused on the effects of various  
106 spatial and temporal types of El Niño events on anthropogenic aerosols, while few  
107 studies have examined their effects on natural aerosols, such as dust, and their  
108 associated mechanisms, which are crucial for predicting and combating dust pollution  
109 in the near future.



110 In this work, the effects of different spatial and temporal types of El Niño on  
111 wintertime and springtime dust pollution in China and the mechanisms behind the  
112 impacts are examined using the Energy Exascale Earth System Model version 1  
113 (E3SMv1). The methods and model description are described in Section 2. The  
114 quantitative impacts of various temporal and spatial types of El Niño events on  
115 wintertime and springtime dust concentrations in China and the associated mechanisms  
116 are elaborated in Section 3. Section 4 summarizes the key results and conclusions of  
117 the study.

118

## 119 **2. Data and Methods**

### 120 **2.1 Data**

121 Global SST patterns and SST anomalies during El Niño events of different  
122 temporal and spatial types are constructed using the merged Hadley-NOAA/OI dataset  
123 which has a horizontal resolution of  $1^\circ \times 1^\circ$  from 1870 to 2017 (Hurrell et al., 2008).  
124 The monthly ERA5 reanalysis data (Hersbach et al., 2020) are applied to evaluate the  
125 simulated meteorological parameters during El Niño events.

126 Hourly observations of  $\text{PM}_{10}$  (particulate matter less than  $10 \mu\text{m}$  in diameter)  
127 concentrations in China from 2015 to 2021 derived from the China National  
128 Environmental monitoring Centre (CNEMC) and the Deep Blue aerosol products  
129 (Platnick et al., 2015) from Moderate Resolution Imaging Spectroradiometer (MODIS)  
130 on Terra satellite, including monthly Aerosol Optical Depth (AOD) at 550 nm and the  
131 Ångström exponent ( $\alpha$ ) from 2001–2020, are applied to evaluate the performance of  
132 dust simulation in the model. The satellite dust optical depth (DOD) is calculated  
133 following Yu et al. (2021).

### 134 **2.2 El Niño events identified as different spatial and temporal types**

135 We first clarify the definition of different temporal and spatial types of El Niño  
136 events here. The notation of year<sup>0</sup> is used to denote the first year of El Niño  
137 development, and Jan<sup>0</sup>, Feb<sup>0</sup>, ..., and Dec<sup>0</sup> indicate the individual months of that year,  
138 while year<sup>1,2,...</sup> and Jan<sup>1,2,...</sup>, Feb<sup>1,2,...</sup>, ..., and Dec<sup>1,2,...</sup>, respectively, denote the  
139 following years and months therein. Niño 3.4 index is defined as the anomaly of  
140 detrended SST in the Niño 3.4 region ( $170^\circ\text{W}$ – $120^\circ\text{W}$ ,  $5^\circ\text{S}$ – $5^\circ\text{N}$ ). Niño 3/4 index  
141 ( $I_{\text{Niño3}}/I_{\text{Niño4}}$ ) is same as Niño 3.4 index, but in the Niño 3/4 region ( $150^\circ\text{W}$ – $90^\circ\text{W}$ ,  $5^\circ\text{S}$ –  
142  $5^\circ\text{N}$ ;  $160^\circ\text{E}$ – $150^\circ\text{W}$ ,  $5^\circ\text{S}$ – $5^\circ\text{N}$ ).



143 For the classification of different temporal types, following Wu et al. (2019), El  
144 Niño events are firstly selected if any of 3-month running averaged Niño 3.4 index  
145 during Oct<sup>0</sup>–Feb<sup>1</sup> greater than 0.75°C. Then the LD El Niño event is identified once  
146 any of Niño 3.4 index during Oct<sup>1</sup>–Feb<sup>2</sup> is higher than 0.5°C; otherwise, it is a SD El  
147 Niño event.

148 Following Yu et al. (2019), the El Niño events, selected with 3-month running  
149 averaged Niño 3.4 indices higher than 0.5°C for five consecutive months, are classified  
150 into different spatial types based on the EP El Niño index ( $I_{EP}$ ) and the CP El Niño index  
151 ( $I_{CP}$ ). The definition of these indices is given below.

$$152 \quad I_{EP} = I_{Ni\tilde{n}o3} - \alpha \times I_{Ni\tilde{n}o4} \quad (1)$$

$$153 \quad I_{CP} = I_{Ni\tilde{n}o4} - \alpha \times I_{Ni\tilde{n}o3} \quad (2)$$

$$154 \quad \alpha = \begin{cases} 0.4, & I_{Ni\tilde{n}o3} \times I_{Ni\tilde{n}o4} > 0 \\ 0, & I_{Ni\tilde{n}o3} \times I_{Ni\tilde{n}o4} \leq 0 \end{cases} \quad (3)$$

155 If the mean  $I_{EP}$  is greater than the  $I_{CP}$  during Oct<sup>0</sup>–Feb<sup>1</sup> of an El Niño, then it is an  
156 EP El Niño event; else, it is a CP El Niño event.

157 The time series of Niño 3.4 index derived from Hadley-NOAA/OI 1870–2017 data  
158 is shown in Figure S1. Using the definitions described above, for El Niño with different  
159 temporal types, 22 SD El Niño events and 8 LD ones are extracted during this time  
160 period; for El Niño with different spatial types, 26 EP El Niño events and 8 CP ones are  
161 extracted.

### 162 **2.3 Model description and experimental design**

163 To investigate the impacts of El Niño of different spatial and temporal types on  
164 dust aerosol in China, this study utilizes the U.S. Department of Energy (DOE)  
165 E3SMv1 (Golaz et al., 2019). As a model developed from the well-known CESM1  
166 (Community Earth System Model version 1), E3SMv1 provides significant  
167 improvements to the atmospheric component, including processes associated with  
168 aerosol, cloud, turbulence, and chemistry (Rasch et al., 2019). We choose the horizontal  
169 resolution of about 1° and 30 vertical layers. E3SMv1 predicts aerosols including  
170 mineral dust, sea salt, sulfate, primary and secondary organic aerosols, and black carbon  
171 in the four-mode Modal Aerosol Module (MAM4) (Wang et al., 2020). E3SMv1  
172 represents dust-related processes in the atmosphere and land model components (Feng  
173 et al., 2022). Dust emissions are calculated at each model time step according to the  
174 wind erosion dust scheme proposed by Zender et al. (2003), which is related to 10-  
175 meter wind speed, surface soil moisture content, soil erodibility, vegetation cover and



176 threshold friction velocity.

177 The following simulations are performed. A “CLIM” experiment applying the  
178 prescribed climatological mean of monthly SST during 1870–2017 is integrated for 30  
179 years. Four sets of sensitivity simulations, “SD”, “LD”, “EP” and “CP”, are driven by  
180 the monthly SST representing the composite of SD, LD, EP and CP El Niño events,  
181 respectively, which is generated through adding the mean monthly SST anomalies from  
182 Jul<sup>0</sup> to Jun<sup>1</sup> of the SD, LD, EP, and CP El Niño events (Fig. S1), respectively, to the  
183 climatological SST between 60°S and 60°N. All the sensitivity experiments have 3  
184 ensemble members with diverse initial conditions branched from different years of the  
185 CLIM simulation. All sensitivity experiments are run for 13 years with the last 10 years  
186 used for analysis. The differences of model fields between the sensitivity simulations  
187 and CLIM represent the influences of El Niño events with different spatial and temporal  
188 types on dust aerosols. All other external factors such as greenhouse gas concentrations,  
189 insolation, anthropogenic aerosols and their precursor emissions are hold at present-day  
190 conditions (year 2014). The SST anomalies relative to the 1870–2017 climatology  
191 during SD, LD, EP and CP El Niño events are shown in Fig. 1.

### 192 **2.3 Model evaluation**

193 To evaluate the model performance in dust simulation, we compare the simulated  
194 near-surface dust concentration and dust optical depth (DOD) over China with observed  
195 PM<sub>10</sub> concentrations and satellite retrieved DOD, respectively. The model can  
196 reproduce the spatial distribution of springtime dust in China, with high dust  
197 concentrations in northwestern China and low in southern and northeastern China (Fig.  
198 S2). The spatial correlation coefficient between the simulated dust concentrations in  
199 E3SMv1 and observed near-surface PM<sub>10</sub> concentrations is +0.55. However, the model  
200 strongly overestimates dust concentrations over the source regions, which were also  
201 reported in many previous studies using the E3SMv1 and CESM (the predecessor of  
202 E3SMv1) (Wang et al., 2020; Wu et al., 2019). The high model bias near the sources is  
203 also confirmed by comparing DOD between model simulation and satellite retrieval. It  
204 suggests that the dust emissions are overestimated in northwestern China in the model.  
205 However, we also note that the E3SMv1 underestimates the transport of dust from  
206 source regions (Wu et al., 2020; Feng et al, 2022), thus the dust over eastern China is  
207 comparable to observations.



## 208 **3. Results**

### 209 **3.1 Impacts of different El Niño types on winter dust pollution**

210 The simulated effects of the four types of El Niño with different spatial positions  
211 (EP and CP) and durations (SD and LD) on the DJF ground-level dust concentrations  
212 are shown in Fig. 2. As for different spatial types of El Niño events, the effects on DJF  
213 dust concentrations in China are similar, with an increase in dust concentrations of 5–  
214  $50 \mu\text{g m}^{-3}$  over central-eastern China during EP and CP El Niño compared to the  
215 climatological means. The spatial pattern of dust changes is consistent with previous  
216 modeling studies (Lee et al., 2015; Li et al., 2021). Although the influences of EP and  
217 CP El Niño on the DJF dust concentrations resemble each other in the spatial patterns  
218 over China, the magnitudes of the influences are different. During CP El Niño relative  
219 to the climatological mean, dust concentrations increase more significantly over  
220 central-eastern China, with the increases of  $20\text{--}50 \mu\text{g m}^{-3}$ ,  $5\text{--}20 \mu\text{g m}^{-3}$  higher than that  
221 during EP El Niño. The large increase during CP El Niño is also more widespread than  
222 that during EP El Niño.

223 As for different temporal types of El Niño events, their effects on DJF dust  
224 concentrations over China are quite different. SD El Niño events cause an increase in  
225 DJF near-surface dust concentrations of  $20\text{--}100 \mu\text{g m}^{-3}$  in northern China and about  $5\text{--}$   
226  $20 \mu\text{g m}^{-3}$  in southern China. Whereas during LD El Niño events, winter dust  
227 concentrations have a decrease of about  $5\text{--}50 \mu\text{g m}^{-3}$  in northern and northeastern China  
228 relative to the climatology and no significant change is shown in southern China. In  
229 contrast to LD El Niño events, SD El Niño events have positive DJF dust concentration  
230 anomalies of  $5\text{--}20 \mu\text{g m}^{-3}$  in southern China and a maximum over  $100 \mu\text{g m}^{-3}$  in  
231 northern China and the Gobi Desert. Furthermore, DJF dust concentrations over the  
232 Taklamakan Desert, one of the largest dust sources in China, have an increase during  
233 LD El Niño events and an insignificant decrease during SD El Niño events.

234 Overall, these changes in dust concentrations indicate that CP El Niño events have  
235 stronger and more widespread impacts on DJF dust concentrations than EP El Niño,  
236 and the SD and LD El Niño events exert opposite impacts on DJF dust in China.

### 237 **3.2 Mechanisms of the different El Niño impacts on winter dust**

238 Meteorological factors such as 10-m wind speed, relative humidity and  
239 atmospheric circulation play a dominant role in altering dust concentrations by altering  
240 emissions, atmospheric transport, and wet scavenging of dust (Csavina et al., 2014).



241 Dust changes are also controlled by the El Niño-related changes in atmospheric  
242 circulation and precipitation (Gong et al., 2006; Hara et al., 2006). The 10-m wind speed,  
243 atmospheric circulation, relative humidity, precipitation anomalies, and related  
244 processes during EP, CP, SD and LD El Niño are investigated here to reveal the  
245 mechanisms of the influence of the four types of El Niño on dust over China.

246 During the CP, EP, and SD El Niño, DJF mean 10-m wind speed increases in the  
247 Gobi Desert and northwestern China compared to the climatological mean (Fig. 3),  
248 which favors the local dust emission over these regions. Whereas for the LD El Niño  
249 event, the positive 10-m wind speed anomaly is greatly weakened, compared to the  
250 other three types of El Niño events, and negative 10-m wind speed anomalies are  
251 triggered in the Gobi Desert and northern China (Fig. 3e), which is not conducive to  
252 dust emission during the LD El Niño events. The CP El Niño events trigger stronger  
253 positive 10-m wind speed anomalies ( $0.1\text{--}0.3\text{ m s}^{-1}$ ) than the EP El Niño events over  
254 the Gobi Desert and northern China (Fig. 3c), which could lead to a greater local dust  
255 emission. Compare to the LD El Niño, SD El Niño events produce significant positive  
256 10-m wind speed anomalies of approximately  $0.3\text{ m s}^{-1}$  in the Gobi Desert and northern  
257 China (Fig. 3f), which is consistent with the increase/decrease in local DJF dust  
258 concentrations during the SD/LD El Niño (Fig. 2). This suggests the importance of 10-  
259 m wind speed in the dust changes during the El Niño events in China.

260 Figure 4 shows the atmospheric circulation anomalies for the four El Niño events.  
261 All types of El Niño have negative anomalies of sea level pressure (SLP) in central-  
262 eastern China, except the LD El Niño that shows a negligible SLP change in winter.  
263 Meanwhile, during the EP, CP, and SD El Niño events, anomalous Mongolian cyclone  
264 can strengthen the local ascending flow to lift more dust particles into the free  
265 atmosphere. The anomalous northwesterly during CP and SD El Niño (Figs. 3b and 3d)  
266 can transport these dust aerosols to central-eastern China, leading to the strong increases  
267 in dust concentrations there (Figs. 2b and 2d). While during the LD El Niño, the lower  
268 atmosphere in the Gobi Desert and northern China is controlled by a weak anomalous  
269 high pressure accompanied by anomalous southeasterly that weakens the prevailing  
270 northwesterly in winter and hinders the vertical lifting and southward transport of dust.

271 Our previous work has confirmed the ability of E3SM in reproducing the  
272 atmospheric circulation in El Niño with different durations (Zeng et al, 2021). Here we  
273 further evaluate the circulations in E3SM simulations during EP and CP El Niño events  
274 by using ERA5 reanalysis data. The anomalous DJF mean 10-m wind speed and 850



275 hPa wind fields in the typical EP El Niño (2006/07) and CP El Niño (2014/15) relative  
276 to the climatology (1950–2017) from ERA5 are presented in Fig. 5. Although the  
277 increase in 10-m wind speed over northwestern China in the EP El Niño simulated in  
278 the model is inconsistent with the ERA5 results, E3SM does capture the large increase  
279 in wind speed over the Gobi Desert during the CP El Niño relative to the climatological  
280 mean and EP El Niño. Moreover, the anomalies in wind fields during EP and CP El  
281 Niño (i.e., anomalous southerly during EP El Niño and anomalous northwesterly during  
282 CP El Niño) are well reproduced by E3SM. It suggests that the atmospheric circulation  
283 features during different types of El Niño are captured by the model. Also note that the  
284 observational differences can be induced by other climate factors besides El Niño,  
285 leading to a potential inconsistency in El Niño impact between model and observation.

286 The effect of relative humidity (RH) on dust concentration is also essential,  
287 considering that a decrease in RH leads to a decrease in the threshold friction velocity  
288 at high RHs (>40%), which further enhances dust emission flux and atmospheric  
289 concentration (Csavina et al., 2014). Both EP and CP El Niño events have negative  
290 anomalies in DJF RH in the Gobi Desert (Figs. 6a and 6b). The decrease in RH reduces  
291 the dust threshold friction velocity and favors dust emission from the Gobi Desert. The  
292 CP El Niño produces more pronounced and widespread negative RH anomalies in the  
293 Gobi Desert and northwestern China than the EP El Niño. It gives approximately 3%  
294 stronger negative RH anomalies (Fig. 6c), resulting in stronger and more widespread  
295 increases in DJF dust concentrations during the CP El Niño event (Fig. 2c). As for El  
296 Niño with different duration, the SD El Niño leads to significant decreases in DJF RH  
297 of about 3% near the south part of the Gobi Desert, while increases in RH are located  
298 over north part of the Gobi Desert during the LD El Niño (Figs. 6g and 6j), likely  
299 resulting in the opposite changes in dust emissions. The ERA5 reanalysis data also  
300 show the same RH variations during the different spatial and temporal types of El Niño  
301 as the E3SM simulations described above (Fig. S3). Among all four types of El Niño  
302 events, RH anomalies are consistent with the distribution of dust concentration  
303 anomalies, which indicates that RH plays an important role in affecting variations in  
304 dust emissions and concentrations in China during El Niño.

305 Fig. 7 shows the simulated changes in DJF dust emissions during different El Niño  
306 events. During the EP and CP El Niño, DJF dust emissions are enhanced in the Gobi  
307 Desert and northwestern China relative to the climatological average. The dust emission  
308 increase is larger during the CP El Niño than the EP El Niño, which is consistent with



309 the higher positive DJF dust concentration anomalies during the CP El Niño.  
310 Furthermore, the SD El Niño causes a significant increase in dust emissions of about  
311  $0.5 \text{ g m}^{-2} \text{ d}^{-1}$  in the Gobi Desert compared to CLIM, while the LD El Niño causes a  
312 decrease in dust emissions. These suggest that different types of El Niño events alter  
313 the DJF dust emissions in China by changing the 10-m wind speed and RH, which is  
314 the important cause of the variation in DJF dust concentrations in China.

315 Furthermore, a reduced DJF precipitation during both EP and CP El Niño events  
316 weakens the wet removal of dust from the atmosphere in northern China (Fig. S4),  
317 further enhancing the increases in DJF dust concentrations.

### 318 **3.3 Spring dust pollution affected by El Niño events**

319 The changes in near-surface dust concentrations over China in the following spring  
320 during the decaying phase for different spatial and temporal types of El Niño are also  
321 examined (Fig. 8). During the following spring, all El Niño events trigger large positive  
322 anomalies of March-April-May (MAM) dust concentrations in northern China.  
323 However, the increases in dust concentrations during the EP, CP and SD El Niño relative  
324 to the climatological average fail the 90% significance test, indicating that the effects  
325 of these types of El Niño events on the dust pollution in northern China in the following  
326 spring are uncertain, likely related to the large internal variability of the climate system.  
327 In contrast to the strong reduction in dust concentrations over the Gobi Desert and  
328 northern China during the LD El Niño in DJF, the effect in MAM reverses to a  
329 significant increase in dust concentrations over these regions by  $50\text{--}100 \mu\text{g m}^{-3}$  (Fig.  
330 8e). It suggests that the weaker intensity but longer duration of LD El Niño than the SD  
331 El Niño can significantly affect spring dust aerosols in China.

332 During LD El Niño events, MAM 10-m wind speed significantly increases over  
333 the Gobi Desert (Fig. S5), which facilitates the local dust emissions, although RH only  
334 shows an insignificant decrease over the dust source region (Fig. S6). It can be  
335 confirmed by the significant increases in MAM dust emissions by about  $0.5 \text{ g m}^{-2} \text{ d}^{-1}$   
336 over the Gobi Desert and northwestern China during LD El Niño events (Fig. 9). Then  
337 the strengthened northwesterly brings more dust to northern China during LD El Niño  
338 events (Fig. S7). Along the transport pathway, the weakened precipitation reduces the  
339 dust wet removal (Fig. S8), leading to the strong increase in MAM dust concentration  
340 over northern China during the LD El Niño.

341



#### 342 **4. Conclusion and discussions**

343 Dust, as an important air pollutant affecting air quality in China in winter and  
344 spring, can be modulated by the interannual variations in El Niño-induced atmospheric  
345 circulation and precipitation anomalies. In this study, the state-of-the-art E3SM model  
346 is used to simulate the effects of different temporal types of El Niño events with short  
347 (SD) and long duration (LD) and different spatial locations of El Niño events with sea  
348 surface temperature anomalies located in Central Pacific (CP) and Eastern Pacific (EP)  
349 on dust concentrations in China.

350 Both CP and EP El Niño events cause 5–50  $\mu\text{g m}^{-3}$  positive anomalies in winter  
351 (DJF months) surface dust concentrations in central-eastern China. Compared to the EP  
352 El Niño, the CP El Niño triggers a stronger wind and negative RH anomalies that lead  
353 to greater local dust emissions. Then the anomalous northwesterly transports the dust  
354 aerosols to central-eastern China during the CP El Niño, accompanied by a reduced  
355 precipitation and wet removal of dust from the atmosphere, resulting in 5–20  $\mu\text{g m}^{-3}$   
356 higher and more widespread DJF dust concentration increases in northern China. For  
357 the different temporal types of El Niño events, wind speed significantly increases over  
358 the Gobi Desert and northern China during the SD El Niño, favoring dust emissions.  
359 Meanwhile, the anomalous northwesterly can increase the transport of dust aerosols to  
360 central-eastern China, leading to an increase in DJF near-surface dust concentrations of  
361 20–100  $\mu\text{g m}^{-3}$  in northern China and 5–20  $\mu\text{g m}^{-3}$  in southern China relative to the  
362 climatological mean. On the contrary, the LD El Niño reduces wind speed over the Gobi  
363 Desert and northern China, which weakens dust emissions, accompanied with the  
364 atmospheric circulation anomalies unfavorable for dust transport, leading to the DJF  
365 dust concentration decrease by 5–50  $\mu\text{g m}^{-3}$  in northern and northeastern China relative  
366 to the climatological mean.

367 In the following spring season, the four types of El Niño events with different  
368 durations and spatial positions all cause positive dust concentration anomalies in  
369 northern China. However, only the changes during the LD El Niño are statistically  
370 significant. This is mainly due to an increase in 10-m wind speed over the Gobi Desert  
371 during the LD El Niño, which enhances the local dust emissions, and then the  
372 strengthened northwesterly brings more dust to the northern China. At the same time,  
373 the weakened precipitation reduces the dust wet removal along the transport pathway.  
374 It suggests that the weaker intensity but longer duration of LD El Niño events than SD



375 El Niño can significantly affect dust aerosols in China in spring.

376 Our results contribute to the current knowledge of the vital influence of different  
377 types of El Niño on dust pollution in winter and spring over China, which have  
378 profound implications for air pollution control and dust storm prediction in China.  
379 Notwithstanding, we also note that the E3SMv1 overestimates dust emissions from the  
380 source regions and underestimates the long-range transport of dust (Wu et al., 2020;  
381 Feng et al, 2022), which may lead to biases in the estimate of El Nino impact on dust  
382 concentrations in China. In future studies, the influences of different types of La Niña,  
383 the cooling phase of ENSO, on dust pollution in China, warrants further investigation.  
384 Besides, other natural aerosols, such as sea salt, are also influenced by El Niño events,  
385 which is not taken into account in this study. In addition to natural sources, dust in  
386 China can also be from anthropogenic emissions (Chen et al., 2019; Xia et al., 2022),  
387 and their relations with El Niño require further study.  
388



389 ***Code and data availability***

390 The E3SMv1 model is available at <https://github.com/E3SM-Project/E3SM> (last access:  
391 25 Mar 2022) (<http://doi.org/10.11578/E3SM/dc.20180418.36>, E3SM project, 2018).

392 Our results can be made available upon request.

393

394 ***Author contributions***

395 YY designed the research and analyzed the data. LZ performed the model simulations.

396 All the authors including HW, PW, and HL discussed the results and wrote the paper.

397

398 ***Competing interests***

399 The authors declare that they have no conflict of interest.

400

401 ***Acknowledgments***

402 HW acknowledges the support by the U.S. Department of Energy (DOE), Office of  
403 Science, Office of Biological and Environmental Research (BER), as part of the Earth  
404 and Environmental System Modeling program. The Pacific Northwest National  
405 Laboratory (PNNL) is operated for DOE by the Battelle Memorial Institute under  
406 contract DE-AC05-76RLO1830.

407

408 ***Financial support***

409 This study was supported by the National Natural Science Foundation of China (grant  
410 41975159), the National Key Research and Development Program of China (grant  
411 2020YFA0607803 and 2019YFA0606800) and Jiangsu Science Fund for Distinguished  
412 Young Scholars (grant BK20211541).



## 413 **References**

- 414 Chen S. Y., Huang J. P., Li J. X., Jia R., Jiang N. X., Kang L. T., Ma X. J., and Xie T.  
415 T.: Comparison of dust emissions, transport, and deposition between the  
416 Taklimakan Desert and Gobi Desert from 2007 to 2011. *Sci. China Earth Sci.*, 60,  
417 1338–1355, <https://doi.org/10.1007/s11430-016-9051-0>, 2017.
- 418 Chen, S., Zhang, X., Lin, J., Huang, J., Zhao, D., Yuan, T., Huang, K., Luo, Y., Jia, Z.,  
419 and Zang, Z.: Fugitive Road Dust PM<sub>2.5</sub> Emissions and Their Potential Health  
420 Impacts, *Environ. Sci. Technol.*, 53, 8455–8465,  
421 <https://doi.org/10.1021/acs.est.9b00666>, 2019.
- 422 Csavina, J., Field, J., Felix, O., Corral-Avitia, A. Y., Saez, A. E., and Betterton, E. A.:  
423 Effect of wind speed and relative humidity on atmospheric dust concentrations in  
424 semi-arid climates, *Sci Total Environ*, 487, 82–90,  
425 <https://doi.org/10.1016/j.scitotenv.2014.03.138>, 2014.
- 426 E3SM Project: Energy Exascale Earth System Model v1.0: Computer Software, DOE  
427 [data set], <https://doi.org/10.11578/E3SM/dc.20180418.36>, 2018.
- 428 Feng, Y., Wang, H., Rasch, P. J., Zhang, K., Lin, W., Tang, Q., Xie, S., Hamilton, D. S.,  
429 Mahowald, N., and Yu, H.: Global dust cycle and direct radiative effect in the  
430 E3SM version 1: Impact of increasing model resolution, *Earth and Space Science*  
431 *Open Archive*, <https://doi.org/10.1002/essoar.10510950.1>, in review for *J. Adv.*  
432 *Model. Earth Sys.*, 2022.
- 433 Golaz, J. C., Caldwell, P. M., Van Roekel, L. P., Petersen, M. R., Tang, Q., Wolfe, J. D.,  
434 Abeshu, G., Anantharaj, V., Asay - Davis, X. S., Bader, D. C., Baldwin, S. A.,  
435 Bisht, G., Bogenschutz, P. A., Branstetter, M., Brunke, M. A., Brus, S. R., Burrows,  
436 S. M., Cameron - Smith, P. J., Donahue, A. S., Deakin, M., Easter, R. C., Evans,  
437 K. J., Feng, Y., Flanner, M., Foucar, J. G., Fyke, J. G., Griffin, B. M., Hannay, C.,  
438 Harrop, B. E., Hoffman, M. J., Hunke, E. C., Jacob, R. L., Jacobsen, D. W., Jeffery,  
439 N., Jones, P. W., Keen, N. D., Klein, S. A., Larson, V. E., Leung, L. R., Li, H. Y.,  
440 Lin, W., Lipscomb, W. H., Ma, P. L., Mahajan, S., Maltrud, M. E., Mametjanov,  
441 A., McClean, J. L., McCoy, R. B., Neale, R. B., Price, S. F., Qian, Y., Rasch, P. J.,  
442 Reeves Eyre, J. E. J., Riley, W. J., Ringler, T. D., Roberts, A. F., Roesler, E. L.,  
443 Salinger, A. G., Shaheen, Z., Shi, X., Singh, B., Tang, J., Taylor, M. A., Thornton,  
444 P. E., Turner, A. K., Veneziani, M., Wan, H., Wang, H., Wang, S., Williams, D. N.,  
445 Wolfram, P. J., Worley, P. H., Xie, S., Yang, Y., Yoon, J. H., Zelinka, M. D., Zender,



- 446 C. S., Zeng, X., Zhang, C., Zhang, K., Zhang, Y., Zheng, X., Zhou, T., and Zhu,  
447 Q.: The DOE E3SM Coupled Model Version 1: Overview and Evaluation at  
448 Standard Resolution, *J. Adv. Model. Earth Sys.*, 11, 2089–2129,  
449 <https://doi.org/10.1029/2018MS001603>, 2019.
- 450 Gong, S. L., Zhang, X. Y., Zhao, T. L., Zhang, X. B., Barrie, L. A., McKendry, I. G.,  
451 and Zhao, C. S.: A Simulated Climatology of Asian Dust Aerosol and Its Trans-  
452 Pacific Transport. Part I: Interannual Variability and Climate, *J. Clim.*, 19, 104–  
453 122, <https://doi.org/10.1175/JCLI3606.1>, 2006.
- 454 Goudie, A. S.: Desert dust and human health disorders, *Environ. Int.*, 63, 101–113,  
455 <https://doi.org/10.1016/j.envint.2013.10.011>, 2014.
- 456 Guo, J., Xu, H., Liu, L., Chen, D., Peng, Y., Yim, S. H.-L., Yang, Y., Li, J., Zhao, C.,  
457 and Zhai, P.: The trend reversal of dust aerosol over East Asia and the North Pacific  
458 Ocean attributed to large-scale meteorology, deposition, and soil moisture. *J.*  
459 *Geophys. Res. Atmos.*, 124, 10450–10466.  
460 <https://doi.org/10.1029/2019JD030654>, 2019.
- 461 Guo, Y., and Tan, Z.: Westward migration of tropical cyclone rapid-intensification over  
462 the Northwestern Pacific during short duration El Nino, *Nat. Commun.*, 9, 1507,  
463 <https://doi.org/10.1038/s41467-018-03945-y>, 2018.
- 464 Hara, Y., Uno, I., and Wang, Z.: Long-term variation of Asian dust and related climate  
465 factors, *Atmos. Environ.*, 40, 6730–6740,  
466 <https://doi.org/10.1016/j.atmosenv.2006.05.080>, 2006.
- 467 Hersbach, H., Bell, B., Berrisford, P., Hirahara, S., Horányi, A., Muñoz-Sabater, J.,  
468 Nicolas, J., Peubey, C., Radu, R., Schepers, D., Simmons, A., Soci, C., Abdalla,  
469 S., Abellan, X., Balsamo, G., Bechtold, P., Biavati, G., Bidlot, J., Bonavita, M.,  
470 Chiara, G. D., Dahlgren, P., Dee, D., Diamantakis, M., Dragani, R., Flemming, J.,  
471 Forbes, R., Fuentes, M., Geer, A., Haimberger, L., Healy, S., Hogan, R. J., Hólm,  
472 E., Janisková, M., Keeley, S., Laloyaux, P., Lopez, P., Lupu, C., Radnoti, G.,  
473 Rosnay, P. de, Rozum, I., Vamborg, F., Villaume, S., and Thépaut, J.-N.: The ERA5  
474 Global Reanalysis, *Q. J. Roy. Meteor. Soc.*, 146, 1999–2049,  
475 <https://doi.org/10.1002/qj.3803>, 2020.
- 476 Huang, J., Wang, T., Wang, W., Li, Z., and Yan, H.: Climate effects of dust aerosols  
477 over East Asian arid and semiarid regions, *J. Geophys. Res. Atmos.*, 119, 11,398–  
478 11,416, <https://doi.org/10.1002/2014JD021796>, 2014.
- 479 Hurrell, J. W., Hack, J. J., Shea, D., Caron, J. M., and Rosinski, J.: A new sea surface



- 480 temperature and sea ice boundary dataset for the Community Atmosphere Model,  
481 J. Clim., 21, 5145–5153, <https://doi.org/10.1175/2008jcli2292.1>, 2008.
- 482 Kao, H-Y., and Yu, J-Y.: Contrasting Eastern-Pacific and Central-Pacific Types of  
483 ENSO, J. Clim., 22, 615–632, <https://doi.org/10.1175/2008jcli2309.1>, 2009.
- 484 Kok, J. F., Ward, D. S., Mahowald, N. M., and Evan, A. T.: Global and regional  
485 importance of the direct dust-climate feedback. Nat. Commun., 9, 241,  
486 <https://doi.org/10.1038/s41467-017-02620-y>, 2018.
- 487 Lee, Y. G., Kim, J., Ho, C.-H., An, S.-I., Cho, H.-K., Mao, R., Tian, B., Wu, D., Lee, J.  
488 N., Kalashnikova, O., Choi, Y., and Yeh, S.-W.: The effects of ENSO under  
489 negative AO phase on spring dust activity over northern China: an observational  
490 investigation, Int. J. Climatol., 35, 935–947, <https://doi.org/10.1002/joc.4028>,  
491 2015.
- 492 Li, J., Garshick, E., Al-Hemoud, A., Huang, S., and Koutrakis, P.: Impacts of  
493 meteorology and vegetation on surface dust concentrations in Middle Eastern  
494 countries, Sci. Total Environ., 712, 136597,  
495 <https://doi.org/10.1016/j.scitotenv.2020.136597>, 2020.
- 496 Li, J., Garshick, E., Huang, S., and Koutrakis, P.: Impacts of El Nino-Southern  
497 Oscillation on surface dust levels across the world during 1982–2019, Sci. Total  
498 Environ., 769, 144566, <https://doi.org/10.1016/j.scitotenv.2020.144566>, 2021.
- 499 Lou, S., Russell, L. M., Yang, Y., Xu, L., Lamjiri, M. A., DeFlorio, M. J., Miller, A. J.,  
500 Ghan, S. J., Liu, Y., and Singh, B.: Impacts of the East Asian Monsoon on  
501 springtime dust concentrations over China, J. Geophys. Res. Atmos., 121, 813 7–  
502 8152, <https://doi.org/10.1002/2016JD024758>, 2016.
- 503 Mao, R., Gong, D., Bao, J., and Fan, Y.: Possible influence of Arctic Oscillation on dust  
504 storm frequency in North China. J. Geogr. Sci. 21, 207–218,  
505 <https://doi.org/10.1007/s11442-011-0839-4>, 2011.
- 506 Platnick, S., Hubanks, P., Meyer, K., and King, M. D.: MODIS Atmosphere L3 Monthly  
507 Product (08\_L3). NASA MODIS Adaptive Processing System, Goddard Space  
508 Flight Center, [http://dx.doi.org/10.5067/MODIS/MOD08\\_M3.006](http://dx.doi.org/10.5067/MODIS/MOD08_M3.006), 2015.
- 509 Rasch, P. J., Xie, S., Ma, P. L., Lin, W., Wang, H., Tang, Q., Burrows, S. M., Caldwell,  
510 P., Zhang, K., Easter, R. C., Cameron-Smith, P., Singh, B., Wan, H., Golaz, J. C.,  
511 Harrop, B. E., Roesler, E., Bacmeister, J., Larson, V. E., Evans, K. J., Qian, Y.,  
512 Taylor, M., Leung, L. R., Zhang, Y., Brent, L., Branstetter, M., Hannay, C.,  
513 Mahajan, S., Mametjanov, A., Neale, R., Richter, J. H., Yoon, J. H., Zender, C. S.,



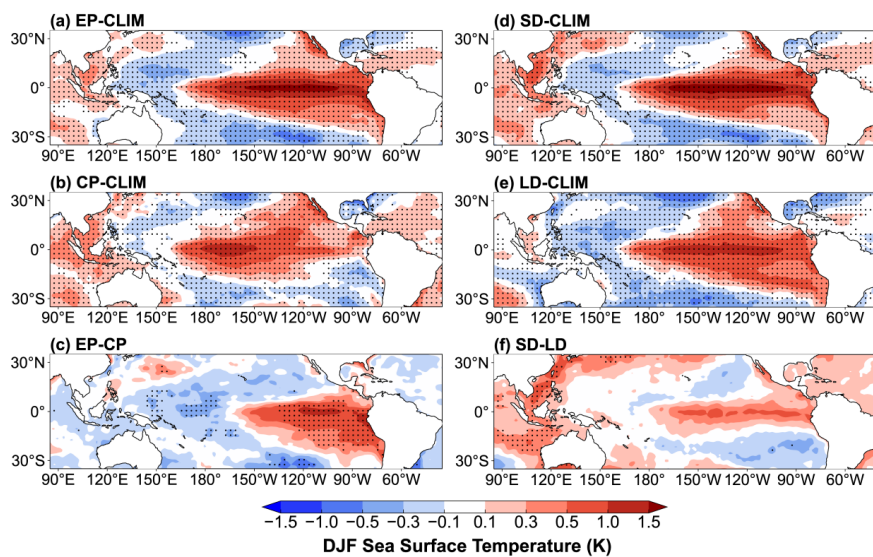
- 514 Bader, D., Flanner, M., Foucar, J. G., Jacob, R., Keen, N., Klein, S. A., Liu, X.,  
515 Salinger, A. G., Shrivastava, M., and Yang, Y.: An Overview of the Atmospheric  
516 Component of the Energy Exascale Earth System Model, *J. Adv. Model Earth Sy.*,  
517 11, 2377–2411, <https://doi.org/10.1029/2019MS001629>, 2019.
- 518 Seinfeld, J. H., Carmichael, G. R., Arimoto, R., Conant, W. C., Brechtel, F. J., Bates, T.  
519 S., Cahill, T. A., Clarke, A. D., Doherty, S. J., Flatau, P. J., Huebert, B. J., Kim, J.,  
520 Markowicz, K. M., Quinn, P. K., Russell, L. M., Russell, P. B., Shimizu, A.,  
521 Shinozuka, Y., Song, C. H., Tang, Y., Uno, I., Vogelmann, A. M., Weber, R. J., Woo,  
522 J.-H., and Zhang, X. Y.: ACE-ASIA: Regional Climatic and Atmospheric  
523 Chemical Effects of Asian Dust and Pollution, *Bull. Am. Meteorol. Soc.*, 85, 367–  
524 380, <https://doi.org/10.1175/BAMS-85-3-367>, 2004.
- 525 Shi, L., Zhang, J., Yao, F., Zhang, D., and Guo, H.: Drivers to dust emissions over dust  
526 belt from 1980 to 2018 and their variation in two global warming phases, *Sci. Total*  
527 *Environ.*, 767, 144806, <https://doi.org/10.1016/j.scitotenv.2020.144860>, 2021.
- 528 Sivakumar M. V.: Impacts of Sand Storms/Dust Storms on Agriculture, in: *Natural*  
529 *Disasters and Extreme Events in Agriculture*, edited by: Sivakumar M.V., Motha  
530 R.P., and Das H.P. Springer, Berlin, Heidelberg, 159–177,  
531 [https://doi.org/10.1007/3-540-28307-2\\_10](https://doi.org/10.1007/3-540-28307-2_10), 2005.
- 532 Trenberth K. E.: The definition of El Niño, *Bull. Am. Meteorol. Soc.*, 78(12), 2771–  
533 2778, [https://doi.org/10.1175/1520-0477\(1997\)078<2771:TDOENO>2.0.CO;2](https://doi.org/10.1175/1520-0477(1997)078<2771:TDOENO>2.0.CO;2),  
534 1997.
- 535 Wang, H., Easter, R. C., Zhang, R., Ma, P.-L., Singh, B., Zhang, K., Ganguly, D., Rasch,  
536 P. J., Burrows, S. M., Ghan, S. J., Lou, S., Qian, Y., Yang, Y., Feng, Y., Flanner,  
537 M., Leung, L. R., Liu, X., Shrivastava, M., Sun, J., Tang, Q., Xie, S., and Yoon, J.-  
538 H., Aerosols in the E3SM Version 1: New developments and their impacts on  
539 radiative forcing, *J. Adv. Model. Earth Sys.*, 12, e2019MS001851,  
540 <https://doi.org/10.1029/2019MS001851>, 2020.
- 541 Wu, M., Liu, X., Yang, K., Luo, T., Wang, Z., Wu, C., Zhang, K., Yu, H., and Darmenov,  
542 A.: Modeling Dust in East Asia by CESM and Sources of Biases, *J. Geophys. Res.*  
543 *Atmos.*, 124, 8043–8064. <https://doi.org/10.1029/2019JD030799>, 2019.
- 544 Wu, M., Liu, X., Yu, H., Wang, H., Shi, Y., Yang, K., Darmenov, A., Wu, C., Wang, Z.,  
545 Luo, T., Feng, Y., and Ke, Z.: Understanding processes that control dust spatial  
546 distributions with global climate models and satellite observations, *Atmos. Chem.*  
547 *Phys.*, 20, 13835–13855, <https://doi.org/10.5194/acp-20-13835-2020>, 2020.



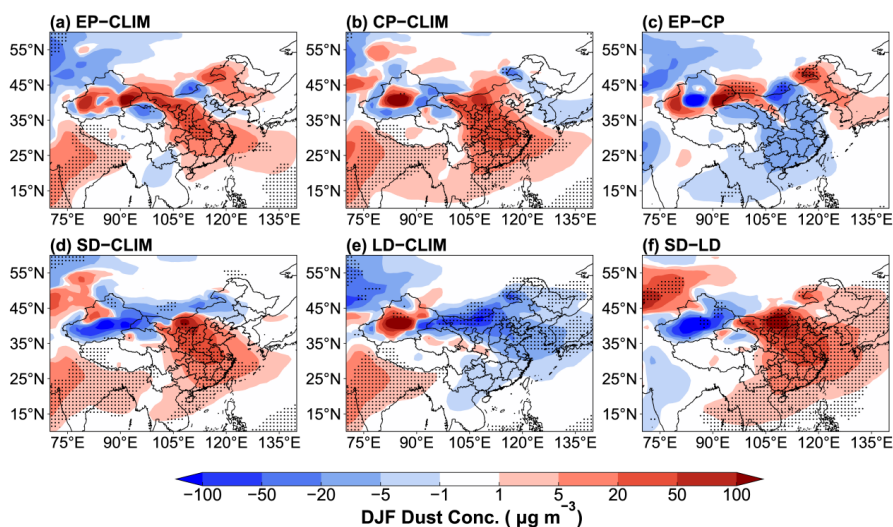
- 548 Wu, X., Okumura, Y. M., and Dinezio, P. N.: What Controls the Duration of El Niño  
549 and La Niña Events?, *J. Clim.*, 32, 5941–5965, [https://doi.org/10.1175/jcli-d-18-](https://doi.org/10.1175/jcli-d-18-0681.1)  
550 0681.1, 2019.
- 551 Xia, W., Wang, Y., Chen, S., Huang, J., Wang, B., Zhang, G. J., Zhang, Y., Liu, X., Ma,  
552 J., Gong, P., Jiang, Y., Wu, M., Xue, J., Wei, L., and Zhang, T.: Double Trouble of  
553 Air Pollution by Anthropogenic Dust, *Environ. Sci. Technol.*, 56, 761–769,  
554 <https://doi.org/10.1021/acs.est.1c04779>, 2022.
- 555 Yang, Y., Russell, L. M., Xu, L., Lou, S., Lamjiri, M. A., Somerville, R. C. J., Miller,  
556 A. J., Cayan, D. R., DeFlorio, M. J., Ghan, S. J., Liu, Y., Singh, B., Wang, H., Yoon,  
557 J.-H., and Rasch, P. J.: Impacts of ENSO events on cloud radiative effects in  
558 preindustrial conditions: Changes in cloud fraction and their dependence on  
559 interactive aerosol emissions and concentrations, *J. Geophys. Res. Atmos.*, 121,  
560 6321–6335, <https://doi.org/10.1002/2015jd024503>, 2016a.
- 561 Yang, Y., Russell, L. M., Lou, S., Liu, Y., Singh, B., and Ghan, S. J.: Rain-aerosol  
562 relationships influenced by wind speed, *Geophys. Res. Lett.*, 43, 2267–2274,  
563 <https://doi.org/10.1002/2016GL067770>, 2016b.
- 564 Yang, Y., Russell, L. M., Lou, S., Liao, H., Guo, J., Liu, Y., Singh, B., and Ghan, S. J.:  
565 Dust-wind interactions can intensify aerosol pollution over eastern China, *Nat.*  
566 *Commun.*, 8, 15333, <https://doi.org/10.1038/ncomms15333>, 2017.
- 567 Yin, Z., Wan, Y., Zhang, Y., and Wang, H.: Why super sandstorm 2021 in North China?,  
568 *Natl. Sci. Rev.*, <https://doi.org/10.1093/nsr/nwab165>, 2021.
- 569 Yu, X., Wang, Z., Zhang, H., and Zhao, S.: Impacts of different types and intensities of  
570 El Nino events on winter aerosols over China, *Sci. Total Environ.*, 655, 766–780,  
571 <https://doi.org/10.1016/j.scitotenv.2018.11.090>, 2019.
- 572 Yu, Y. and Ginoux, P.: Assessing the contribution of the ENSO and MJO to Australian  
573 dust activity based on satellite- and ground-based observations, *Atmos. Chem.*  
574 *Phys.*, 21, 8511–8530, <https://doi.org/10.5194/acp-21-8511-2021>, 2021.
- 575 Zender, C. S., Bian, H., and Newman, D.: Mineral Dust Entrainment and Deposition  
576 (DEAD) model: Description and 1990s dust climatology, *J. Geophys. Res.*, 108,  
577 4416, <https://doi.org/10.1029/2002JD002775>, 2003.
- 578 Zeng, L., Yang, Y., Wang, H., Wang, J., Li, J., Ren, L., Li, H., Zhou, Y., Wang, P., and  
579 Liao, H.: Intensified modulation of winter aerosol pollution in China by El Niño  
580 with short duration, *Atmos. Chem. Phys.*, 21, 10745–10761,  
581 <https://doi.org/10.5194/acp-21-10745-2021>, 2021.



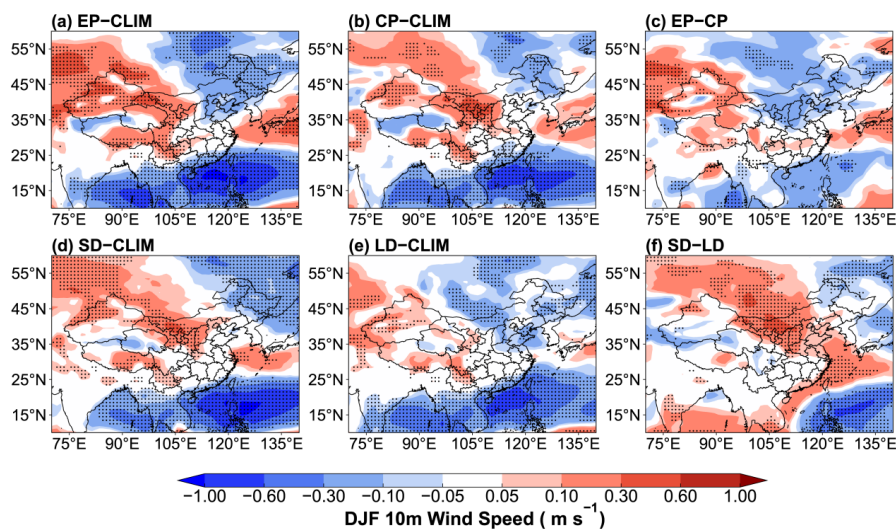
- 582 Zhao, S., Zhang, H., and Xie, B.: The effects of El Niño-Southern Oscillation on the  
583 winter haze pollution of China, *Atmos. Chem. and Phys.*, 18, 1863–1877,  
584 <https://doi.org/10.5194/acp-18-1863-2018>, 2018.
- 585 Zhu, C., Wang, B., and Qian, W.: Why do dust storms decrease in northern China  
586 concurrently with the recent global warming?, *Geophys. Res. Lett.*, 35, L18702,  
587 <https://doi.org/10.1029/2008GL034886>, 2008.
- 588



589  
590 **Figure 1.** Composite differences in DJF mean SST ( $^{\circ}\text{C}$ ) between (a) EP, (b) CP, (d) SD, (e) LD El  
591 Niño events and climatological mean over 1870–2017, and (c) between EP and CP, and (f) between  
592 SD and LD El Niño events. Statistically significant differences at 98% from a two-tailed T-test are  
593 stippled.  
594



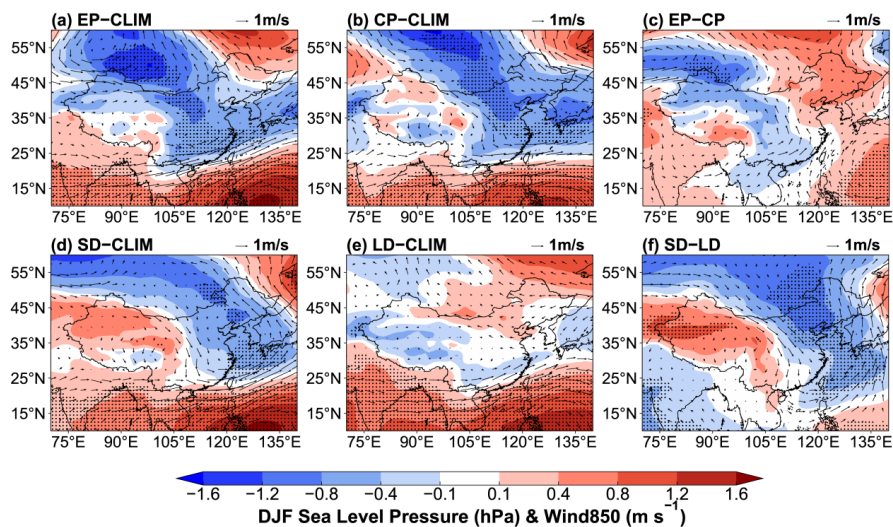
595  
596 **Figure 2.** Composite differences in DJF mean near-surface dust concentrations ( $\mu\text{g m}^{-3}$ ) between  
597 EP and CLIM in (a), CP and CLIM in (b), EP and CP in (c), SD and CLIM in (d), LD and CLIM in  
598 (e), and SD and LD in (f). The stippled areas indicate statistical significance with 90% confidence  
599 from a two-tailed T-test.  
600



601  
602 **Figure 3.** Composite differences in DJF mean 10-m wind speed ( $\text{m s}^{-1}$ ) between EP and CLIM in  
603 (a), CP and CLIM in (b), EP and CP in (c), SD and CLIM in (d), LD and CLIM in (e), and SD and  
604 LD in (f). The stippled areas indicate statistical significance with 90% confidence from a two-  
605 tailed T-test.  
606



607



608

609

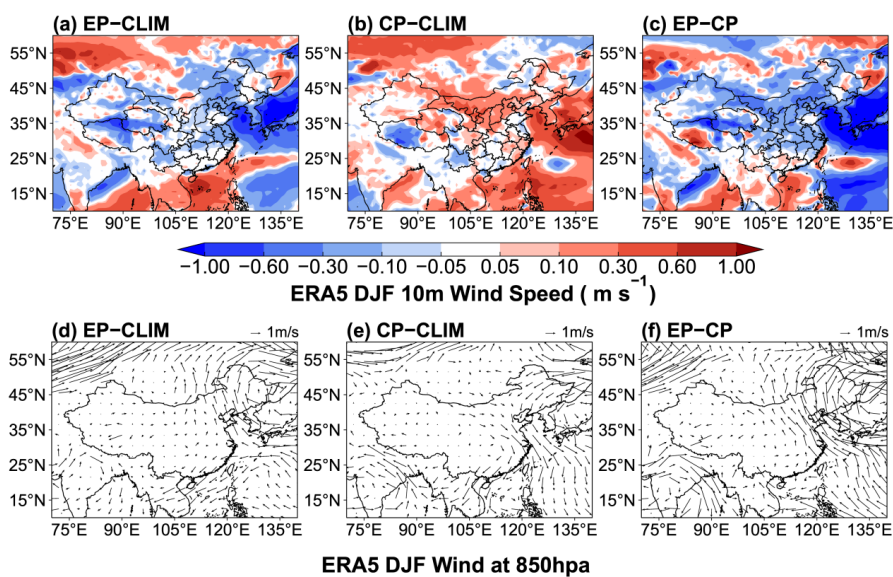
610

611

612

613

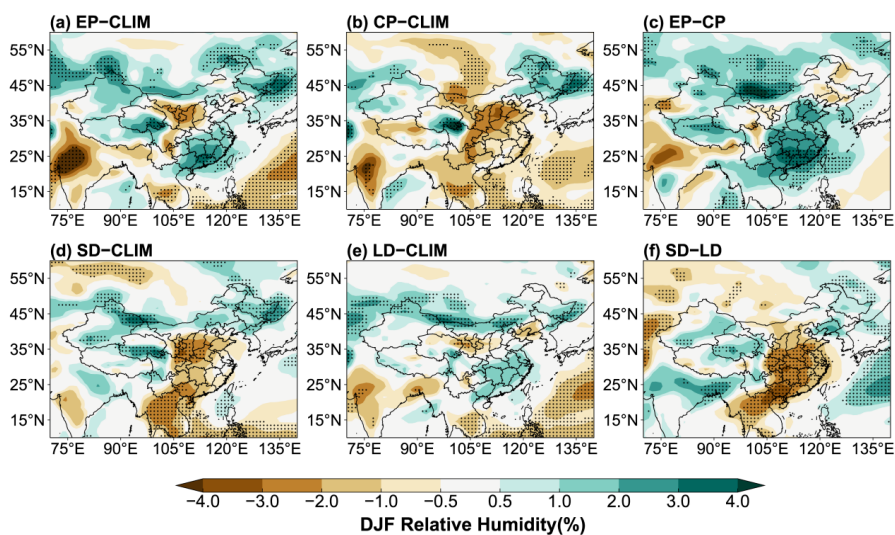
**Figure 4.** Composite differences in DJF mean sea level pressure (SLP, shaded; units: hPa) and winds at 850 hPa (WIND850, vector; units:  $\text{m s}^{-1}$ ) between EP and CLIM in (a.), CP and CLIM in (b), and EP and CP in (c), SD and CLIM in (d), LD and CLIM in (e), and SD and LD in (f). The stippled areas indicate statistical significance with 90% confidence from a two-tailed T-test.



614

615 **Figure 5.** Composite differences in DJF mean 10-m wind speed ( $\text{m s}^{-1}$ ) (top panels) and wind at 850  
616 hPa (vector; units:  $\text{m s}^{-1}$ ) (bottom panels) between 2006/07 EP El Niño and climatological mean  
617 (1950–2017) in (a, d), 2014/15 CP El Niño and climatological mean in (b, e), and 2006/07 EP El  
618 Niño and 2014/15 CP El Niño in (c, f) from the ERA5 reanalysis data. The data were detrended over  
619 1950–2017.

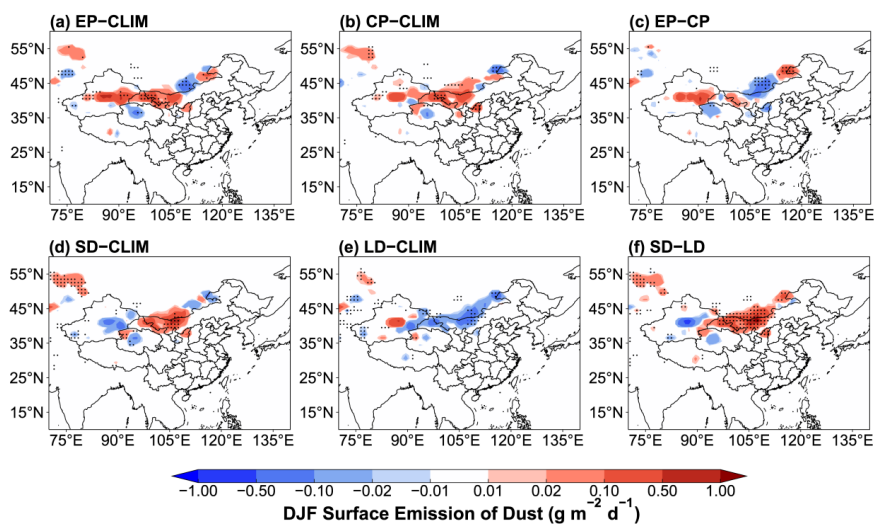
620



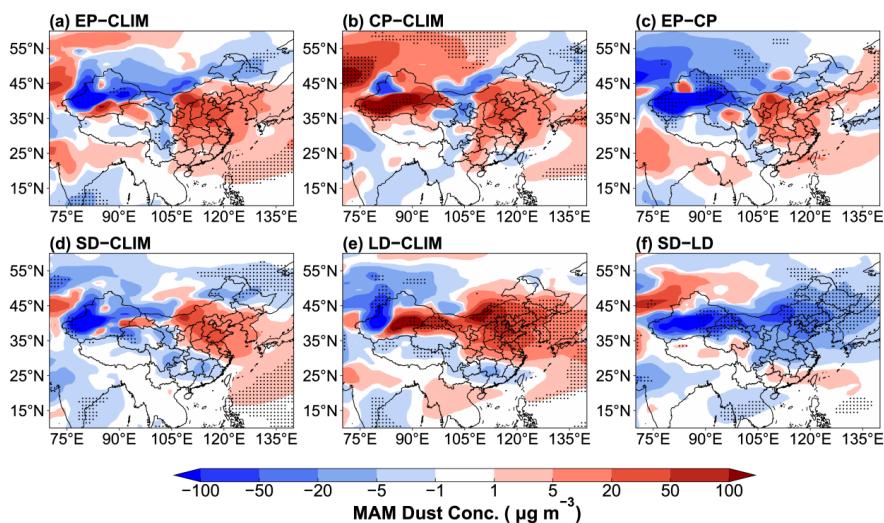
621

622 **Figure 6.** Composite differences in DJF mean relative humidity (units: %) between EP and CLIM  
623 in (a), CP and CLIM in (b), and EP and CP in (c), SD and CLIM in (d), LD and CLIM in (e), and  
624 SD and LD in (f). The stippled areas indicate statistical significance with 90% confidence from a  
625 two-tailed T-test.

626



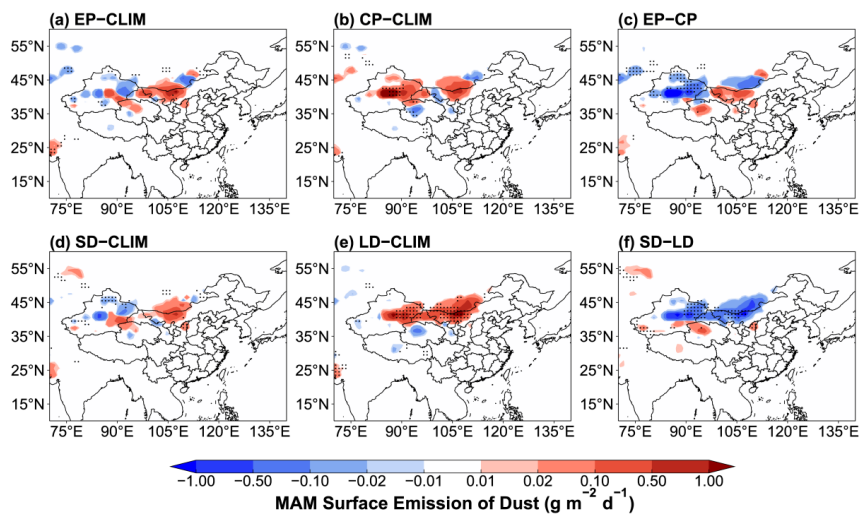
627  
628 **Figure 7.** Composite differences in DJF mean dust emissions ( $\text{g m}^{-2} \text{d}^{-1}$ ) between EP and CLIM in  
629 (a), CP and CLIM in (b), EP and CP in (c), SD and CLIM in (d), LD and CLIM in (e), and SD and  
630 LD in (f). The stippled areas indicate statistical significance with 90% confidence from a two-tailed  
631 T-test.  
632



633  
634 **Figure 8.** Composite differences in MAM mean near-surface dust concentrations ( $\mu\text{g m}^{-3}$ ) between  
635 EP and CLIM in (a), CP and CLIM in (b), EP and CP in (c), SD and CLIM in (d), LD and CLIM in  
636 (e), and SD and LD in (f). The stippled areas indicate statistical significance with 90% confidence  
637 from a two-tailed T-test.  
638



639



640

641

642

643

644

645

**Figure 9.** Composite differences in MAM mean dust emissions ( $\text{g m}^{-2} \text{d}^{-1}$ ) between EP and CLIM in (a), CP and CLIM in (b), EP and CP in (c), SD and CLIM in (d), LD and CLIM in (e), and SD and LD in (f). The stippled areas indicate statistical significance with 90% confidence from a two-tailed T-test.